

Rate-dependent ferroelectric switching in barium titanate ceramics from modified PUND experiments

Vignesh Kannan*, Dennis M. Kochmann

Mechanics & Materials Lab, Department of Mechanical and Process Engineering, ETH Zürich, 8092 Zürich, Switzerland

ARTICLE INFO

Article history:

Received 18 July 2022

Received in revised form 25 August 2022

Accepted 28 September 2022

Available online xxxx

Dataset link: <https://doi.org/10.3929/ethz-b-000558108>

Keywords:

Ferroelectricity

Rate dependence

Domain switching

In-situ experiments

ABSTRACT

Predicting and controlling the rate-dependent electro-mechanical switching in ferroelectric ceramics is challenging due to our current lack of understanding the underlying domain switching mechanisms at short time scales or high rates. Therefore, we propose an experimental protocol, which is a modification of the so-called Positive Up Negative Down (or PUND) experiment, to probe the rate-dependent competition between domain nucleation, domain growth, and variant selection in barium titanate ceramics as a representative material. Our experiments use a *pump* electric field pulse to switch the sample from a poled state at electric field rates spanning five orders of magnitude ($10^{-2} - 10^2$ MV/m·s). The remanent microstructures at the end of different pump pulses are probed using a subsequent *probe* electric field pulse, which is applied at a constant quasistatic rate. Results reveal reduced polarizability at higher electric field rates, indicating reduced domain switching. In addition, this pump-probe experiment shows an increase in domain wall nucleation vs. growth at higher rates. Simultaneous mechanical strain measurements using stereographic digital image correlation indicate a difference in nucleated domain wall variants while switching anti-parallel vs. parallel to the pre-poled direction. The data shows that ferroelastic 90° domain nucleation is preferred in the former case, while ferroelectric 180° nucleation is preferred in the latter. Our study highlights the importance of quantifying microscopic kinetics of domain nucleation, domain wall growth, and the effect of mobile defects in modeling the short-time electro-mechanical response of ferroelectric ceramics.

© 2022 The Author(s). Published by Elsevier Ltd. This is an open access article under the CC BY license (<http://creativecommons.org/licenses/by/4.0/>).

1. Introduction

As a popular class of active materials, ferroelectrics are ubiquitous across technological applications including infrared detection [1,2], energy harvesting [3–5], acoustics, sensors, transducers [6], active structures [7–11], electro-optics [12], and more recently in nanoscale devices for memory storage [13–15] and electronics [16,17]. At the core of this multi-functionality is the coupling between thermal, electrical, and mechanical fields inside the material.

In crystalline ferroelectrics, the origin of this multi-physical coupling lies in a non-centrosymmetric atomic structure, resulting in a permanent electric dipole moment below a material's Curie temperature [18]. Upon application of large electric fields a reversal of polarization occurs by the heterogeneous nucleation and growth of nano- to micron-scale domains of constant dipole moment, separated by interfaces known as domain walls (DWs) [19]. This process is dissipative and sensitive to the time

scale of loading, which results in rate-dependent material behavior. While limited efforts to understand these rate effects have been undertaken in bulk ferroelectric ceramics [20–22], our knowledge of their physical origins has remained incomplete, among others since very few studies have explored time scales smaller than seconds [20,23–26]—especially in lead-free barium titanate ceramics [27–29]. Besides limiting our physical understanding, this also limits our ability to accurately model the material (and device) performance at short time scales.

The rate dependence of the macroscopic thermo-electromechanical response emerges from the collective nucleation and growth of DWs [30–32]. The *kinetics* – i.e., the rates of nucleation and growth of DWs as functions of the thermodynamic driving forces on the DWs [33–35] – are poorly understood, especially at short time scales. Direct observation of DW kinetics, especially in *ceramics* as opposed to single-crystals, using *in-situ* experiments are complex, often requiring expensive, large-scale experimental facilities [27,29,32,36,37]. At macroscopic length scales, cyclic hysteresis experiments offer limited insight into the kinetics of polarization switching due to two effects: (i) the lack of direct measurements of polarization (as opposed to electric displacement), and (ii) history dependence of DW nucleation and growth.

* Corresponding author.

E-mail addresses: kannanv@ethz.ch (V. Kannan), dmk@ethz.ch (D.M. Kochmann).

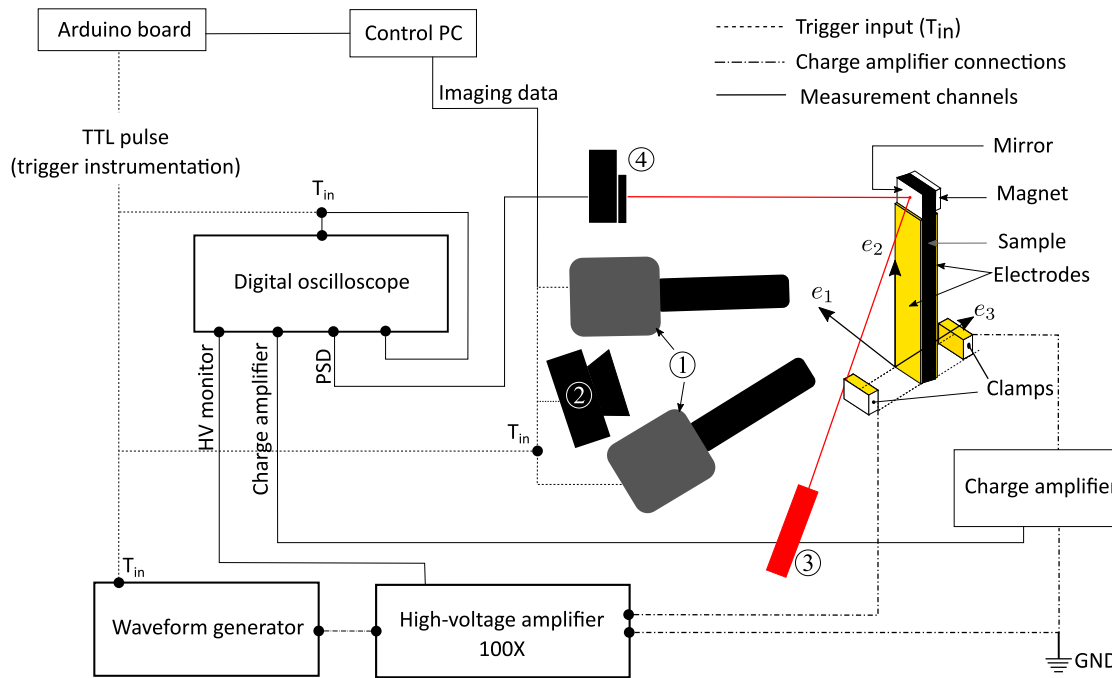


Fig. 1. Schematic of the Broadband Electromechanical Spectroscopy (BES) experiment. ① Stereo-camera setup for Digital Image Correlation; ② Pulsed imaging light source; ③ 633 nm He-Ne laser source; ④ 2-D position sensing detector (PSD); GND represents the ground.

In this study, we explore the effects of the rate of the applied electric field on polarization switching in ferroelectric ceramics using *in-situ* laboratory-scale experiments using barium titanate (BaTiO_3) as a model material. Our experiments allow for the simultaneous measurement of electric displacement and spatially-resolved mechanical strains during the application of large-amplitude electric fields across a range of time scales spanning five orders of magnitude. By modifying a sequential switching experiment, commonly abbreviated as PUND (Positive Up Negative Down) [38], we isolate polarization switching and strains due to DW kinetics alone. The combination of macroscopic electrical and mechanical measurements *in-situ* offers a unique and simple method to probe the competition between nucleation and growth of different types of ferroelectric domains across time scales.

2. Materials and methods

2.1. Materials

Samples of commercially manufactured 3%-doped BaTiO_3 ceramic (DeL Piezo Specialties, LLC, U.S.A.) were pre-poled, and silver electrodes were fired on the front and back 40 mm × 3 mm surfaces of the samples. Preliminary EDS (Electron Dispersive Spectroscopy) analysis showed that the primary dopant was Ca^{2+} (~1.7 at.%). Scanning Electron Microscopy (SEM) imaging revealed grain sizes on the order of 3 μm , while the initial polarization state of a sample before cycling is generally unknown.

2.2. Experimental setup

We use a custom-built experimental setup named Broadband Electromechanical Spectroscopy (BES) [39], originally developed to study viscoelasticity in ferroelectric ceramics [11]. The sample geometry is a cantilever beam of dimensions 40 mm × 3 mm × 1 mm, mounted between custom-designed Macor clamps with

glued copper tape (see Fig. 1). The copper electrodes are connected to a high-voltage amplifier (Trek 10/10B-HS), capable of maximum output voltages of $\pm 10 \text{ kV}$ with a slew rate of 700 V/ μs and bandwidth of 20 kHz. Electric fields were applied to the sample through high-voltage cables soldered to electrodes on the Macor clamps, using a function generator (Tektronix AFG31022), amplified by a constant gain of 1000 V/V. The electric displacement across the sample was measured using an in-house charge amplifier circuit with a gain of 10^5 [40]. Mechanical strains were measured by stereoscopic digital image correlation (stereo-DIC). Two cameras (Basler acA 4112; resolution: 4096 × 3000 pixels; pixel (px) size 3.5 μm) were mounted at an angle of $\sim 15^\circ$ with respect to each other. Camera optics were chosen to achieve lateral resolutions of $\sim 4 \mu\text{m}$ per pixel. Correlation-based displacement calculations were performed using the commercial code Vic-3D (Correlated Solutions). The field of view achieved by the optics was approximately 20 mm × 3 mm. A suitable region of interest (ROI) within this field of view was chosen to be at least 5 mm × 2 mm, such that the signal-to-noise ratio of captured images was well-suited for correlation and statistically significant strain measures were extracted for each experiment, while decreasing the noise due to numerical differentiation of displacement data. For the displacement correlation, a subset size of ~ 100 –150 px was chosen with a step size of ~ 21 px, thus ensuring on the order of 10^3 data points per experiment. Strains were calculated from displacement data using a filter size of ~ 300 –400 px. To determine the mean and standard deviations of time-resolved strain fields, the edges of the ROI were ignored due to potential errors during numerical differentiation. All instrumentation and data acquisition were controlled remotely using a Python script. All experiments were performed at room temperature.

2.3. Experimental protocol: From classical PUND to our modified pump-probe experiment

Typical experiments to probe the hysteretic effects of ferroelectric switching are based on a cyclic electrical loading history.

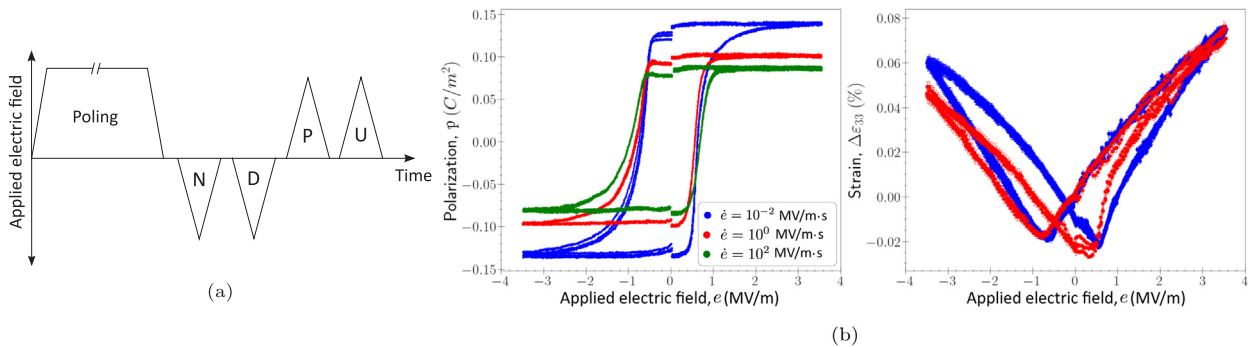


Fig. 2. Conventional PUND experiments to probe rate effects: (a) schematic of the electrical loading sequence of a single PUND experiment; (b) data from three different loading rates covering five orders of magnitude, showing the total polarization and through-thickness strain vs. applied electric field.

This has, however, one significant limitation: the charge amplifier measures the electric displacement d and not the polarization p of the sample [41]. In a perfectly insulating ferroelectric material, electric displacement changes occur due to a combination of the dielectric effect and polarization switching (through domain evolution). In addition, leakage currents due to the finite electrical conductivity may occur, especially in thin films [42]. The PUND (Positive Up Negative Down) experiment was introduced to eliminate those effects and hence to measure the electrical hysteresis due to polarization/domain switching alone. It has become a mainstream characterization protocol for thin-film ferroelectrics and antiferroelectrics [38,43–46].

Our experimental protocol applies five sequential electric field pulses to a sample (see Fig. 2(a)). The first pulse, called a *poling* pulse, applies a constant electric field over an extended period of time such as to induce complete switching. This also defines the *positive* direction for subsequent applied electric fields, while applying a subsequent electric field in the opposite direction is referred to as *negative*. We align the positive direction with the pre-poled direction indicated by the manufacturer. The second pulse, called a *switching* pulse, switches the polarization in the direction opposite to the initial poling (at a chosen rate). The measured response includes polarization evolution due to domain switching, the volume-averaged dielectric effect, and leakage currents (for lossy samples). In our experiments, we call this the 'N' (negative) pulse. Classical PUND measurements assume a complete reorientation of the sample polarization (saturation) during this switching step—an assumption that we cannot make due to limited switching with increasing loading rates (as we will demonstrate later). The third pulse, also referred to as a *non-switching* pulse, is in the same (negative) direction and probes the leakage and dielectric effect of the final state from the previous N pulse. This is labeled as the 'D' (down) pulse. By subtracting the electrical displacement data between the N and D pulses, the time-resolved polarization of the sample is calculated for the negative direction. A similar sequence follows in pulses four and five, which switch the sample in the positive direction through the 'P' (positive) and 'U' (up) pulses. This allows for a full reconstruction of the $p-e$ -hysteresis loop, as opposed to the $d-e$ -loop measured from a cyclic electric field history. Labels N, D, P, and U are used throughout this manuscript to define the four pulses.

To investigate the effects of the *rate* of the applied electric field on polarization switching, a modification of the PUND experiment was necessary, as incomplete switching occurs during the switching pulses (N and P) at higher rates [40]. Consequently, the D and U pulses can no longer be considered as *non-switching*. A schematic of the modified PUND sequence is shown in Fig. 3(a). While the switching pulses (N and P) are performed across a range of rates with time scales spanning six orders of magnitude, the subsequent D and U pulses are maintained at the lowest rate

(7×10^{-3} MV/m·s). This choice is based on two assumptions: (i) the lowest rate of the applied electric field is assumed to be quasistatic, i.e., domains evolve under equilibrium conditions, and (ii) the amplitude of the applied electric field is sufficiently high such that complete switching is achieved at the quasistatic rate. Consequently, the N and P pulses in the modified PUND sequence are *pump* pulses that drive polarization switching at different rates from consistent initial conditions, whereas the D and U pulses are *probe* pulses that allow the remanent polarization to evolve quasistatically. That is, while the N and P pulses are expected to switch the ferroelectric ceramics to varying degree (based on the rate of applied electric field and intrinsic switching kinetics), the subsequent D and U pulses "perform the remaining switching" to the final equilibrium configuration under quasistatic conditions. We refer to the rate of applied external electric field \dot{e} as the *electric field loading rate* throughout this study. This terminology allows us to clearly differentiate between initial and boundary conditions on the sample and internal electric fields developed during switching.

Note that this is different from conventional pump-probe experiments, widely used to measure dynamic phenomena in materials (see e.g., [47–51]). In those experiments, the pump drives the relevant dynamic phenomena, while the probe measures the dynamics *non-destructively*. In our experiments, however, the *probe* measures the remanent state *destructively* i.e., by modifying the remanent polarization state quasi-statically—thus decoupling intrinsic kinetics and history effects.

2.4. Pre-conditioning: Poling step

In-situ investigations of the absolute polarization state of the sample are complex and may require specialized facilities. Instead, we applied a pre-poling step, which achieves peak electric fields of 3.5 MV/m (beyond which electric arcing occurs around the sample, as the experimental geometry does not allow for immersing the entire sample in a medium of high dielectric strength like silicone oil). By performing the pre-poling step at the peak electric field over long times (at least 10^3 seconds), we ensure consistent initial configurations for every measurement. As the coercive fields reported for BaTiO₃ [52] are significantly lower than the peak applied electric field, we assume that samples are close to being fully poled at the start of each measurement.

2.5. Extraction of polarization and switching strain from experimental data

The electric displacement vector \mathbf{d} is linked to the electric field vector \mathbf{e} and the polarization vector \mathbf{p} (all being functions

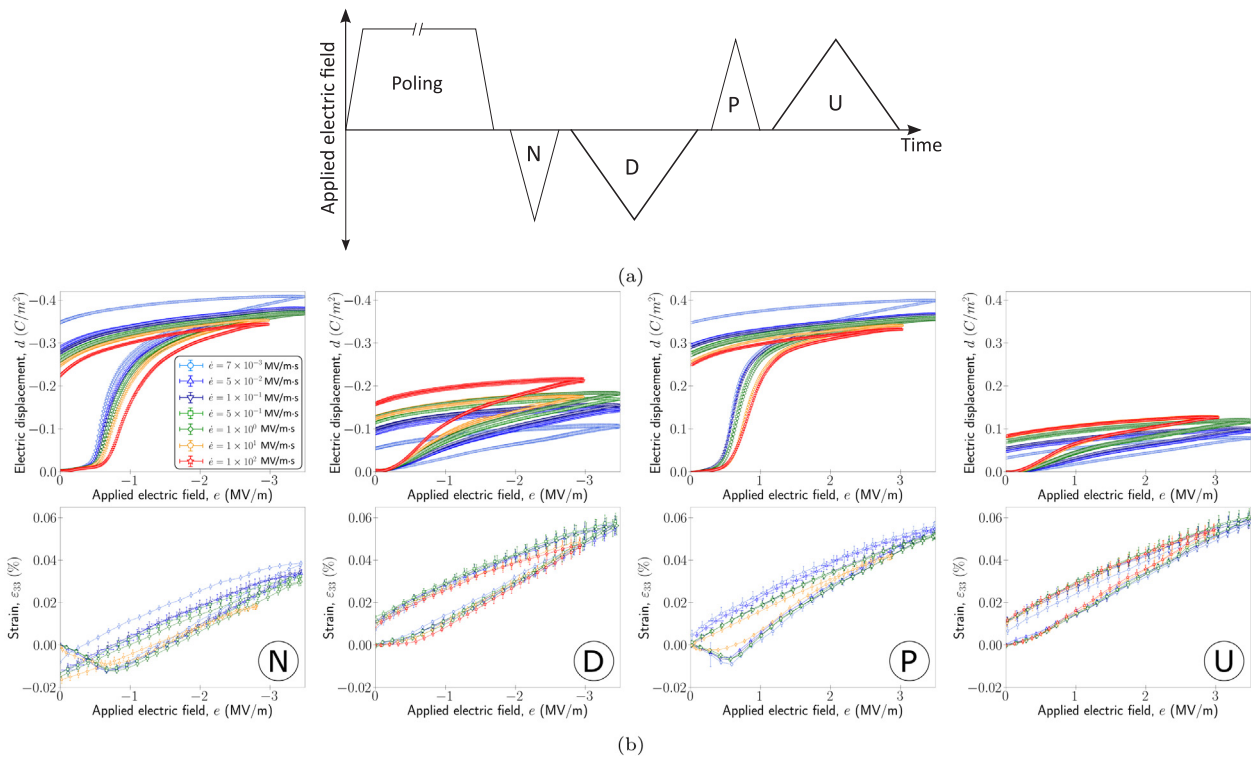


Fig. 3. Modified PUND experiment to probe rate-dependent electro-mechanical switching: (a) schematic of the electric loading pulses. N and P are pump pulses at constant high rates, while D and U pulses probe the remanent polarization at a constant quasistatic rate; (b) experimental data obtained from the modified PUND sequence across five orders of magnitude in electrical loading rate. Rates here refer to the magnitude of \dot{e} during the N and P pump pulses.

of position \mathbf{x} within the sample and time t) via the constitutive relation

$$\mathbf{d}(\mathbf{x}, t) = \epsilon \mathbf{e}(\mathbf{x}, t) + \mathbf{p}(\mathbf{x}, t), \quad (1)$$

where ϵ is the permittivity tensor in vacuum. The volume average of these spatially-resolved quantities is defined as

$$\langle \cdot \rangle = \frac{1}{V} \int_{\mathcal{V}} (\cdot)(\mathbf{x}) dV \quad \Rightarrow \quad \langle \mathbf{d}(\mathbf{x}, t) \rangle = \epsilon \langle \mathbf{e}(t) \rangle + \langle \mathbf{p}(\mathbf{x}, t) \rangle, \quad (2)$$

where \mathcal{V} refers to the region of interest, and V is its volume. From an experimental perspective, additional leakage effects in the form of sample resistance are inevitable due to charge defects in the sample. Hence, the scalar form of Eq. (1), along the \mathbf{e}_3 -direction of the applied electric field, may be rewritten as

$$\langle d_3 \rangle = \epsilon_{33} \langle e_3 \rangle + \langle p_3 \rangle + d^{\text{leakage}}, \quad (3)$$

where $e = \langle e_3 \rangle$ is the applied electric field through the specimen thickness, $d = \langle d_3 \rangle$ is the measured electric displacement across the thickness, and the last term is due to leakage currents.

The study of leakage currents and their rate effects are beyond the scope of this study. Literature evidence has pointed to multiple mechanisms for leakage (see, e.g., [42]). Current-voltage data in thin films shows a linear ohmic response at small electric fields, and a nonlinear response at larger fields. This is significant primarily in thin films with thicknesses on the order of nanometers [38,42,53].

Bulk ceramic samples are less susceptible to leakage effects. Our hysteresis data (reported in [40]) qualitatively show that leakage current effects are minimal [52]. A simple calculation yields the effect of a linear conductivity on the charge accumulation in our samples, assuming a linear ohmic response [54], as

$$d(t) = \frac{1}{A} \int_0^t i(t) dt = \frac{h}{A} \int_0^t \Omega e(t) dt, \quad (4)$$

where i and d are, respectively, the leakage currents and electric displacements, A and h are the cross-sectional area and thickness of the sample, respectively. Ω is the conductivity of the sample, and $e(t)$ is the applied electric field history as a function of time t . By inserting the parameters from our quasistatic experiments ($\dot{e} = 7 \times 10^{-3} \text{ MV/m s}$), we calculate an upper limit for d as $2.4 \times 10^{-2} \text{ C/m}^2$, which is an order of magnitude smaller than our measurements for the pump pulses (preliminary resistance measurements show values on the order of 10^{11} Ohm). At higher rates, these values are significantly smaller. Note that leakage in bulk ceramics occurs by the migration of extrinsic charged defects in the material [55]. These are linked to the kinetics of domains and may result in a non-ohmic response. For the pump pulse data we interpret domain wall kinetics in conjunction with the kinetics of charged defects. The leakage effects, if any, are eliminated for the probe pulses, as all probe data were collected at the same rate.

To extract the through-thickness polarization $p = \langle p_3 \rangle$ from electric displacement data, we revisit the second assumption discussed above (i.e., that the amplitude of the applied electric field is sufficiently high so complete switching is achieved at quasistatic rates). Consequently, the first and third terms in Eq. (3) can be calculated from the data of the probe pulses D and U, following complete switching at the lowest rates (identified by the superscript (0)). The polarization at different rates can hence be calculated from the experimental data by comparing measured electric displacements at different rates \dot{e} but at the same electric field e :

$$p|_{e, \dot{e}} = d|_{e, \dot{e}} - d|_{e, \dot{e}=\dot{e}^{(0)}}. \quad (5)$$

While some residual polarization due to incomplete switching may be expected, especially in polycrystalline doped samples, this contribution is small compared to the spontaneous polarization. In addition, this polarization is reversible, i.e., it is recovered upon removal of the electric field and hence does not play a role

in switching. We reiterate that the correction shown in Eq. (5) was applied to data along each direction separately, hence $\dot{\epsilon}$ is interpreted as the magnitude of the electric field loading rate.

Analogously, the constitutive equation for the mechanical actuation strain reads

$$\langle \boldsymbol{\epsilon}(\mathbf{x}, t) \rangle = \langle \mathcal{D}(\mathbf{x}, t) \boldsymbol{\epsilon}(t) \rangle + \langle \boldsymbol{\epsilon}^t(\mathbf{x}, t) \rangle \quad (6)$$

where $\boldsymbol{\epsilon}$ is the symmetric second-order strain tensor, \mathcal{D} the piezoelectric tensor, and $\boldsymbol{\epsilon}^t$ a transformation strain tensor that accounts for strains due to domain switching. In tetragonal crystal systems such as BaTiO₃ at room temperature, two types of DWs exist—ferroelectric (180°) and ferroelastic (90°). The former are characterized by a jump in only the electric dipole moment, while the latter are characterized by jumps in both dipole moment and mechanical strain. The strain data allows us to decouple the contribution of ferroelastic domains from macroscopic polarization switching.

If one were to assume that the effective piezoelectric tensor of the polycrystalline sample is approximately constant throughout the switching process (i.e., $\langle \mathcal{D}(\mathbf{x}, t) \rangle \approx \mathcal{D} = \text{const.}$), then – in analogy to Eq. (5) – the transformation strain $s = \langle \epsilon_{33}^t \rangle$ due to polarization switching can be calculated (again evaluated at different rates but the same electric field) as

$$s|_{e,\dot{\epsilon}} = s|_{e,\dot{\epsilon}} - s|_{e,\dot{\epsilon}=\dot{\epsilon}^{(0)}}. \quad (7)$$

Unfortunately, the anisotropy in the piezoelectric tensor is so large ($d_{33}/d_{31} > 2.5$) [18] that this assumption does not apply. The evolution of transformation strains due to polarization switching cannot be tracked *in-situ* using purely macroscale experiments. A useful metric used in this study is the remanent strain, Δs , which is a measure of incomplete ferroelastic domain switching during a pulse and defined as the difference in average strain before and after a pulse (for any loading rate), i.e.,

$$\Delta s|_{\dot{\epsilon}} = \langle \epsilon \rangle|_{t=t_p} - \langle \epsilon \rangle|_{t=t_0} \quad (8)$$

where t_0 and t_p are the start and end times of a pulse, respectively.

3. Results and discussion

We present two sets of experiments on bulk polycrystalline BaTiO₃ ceramics across a range of time scales spanning five orders of magnitude, using both the conventional PUND sequence and a modified PUND sequence. The former experiments, while presenting rate-dependent switching kinetics on the macroscopic scale, were found to be inadequate to interpret the underlying domain nucleation and growth kinetics, and hence a majority of our study focuses on the latter. A poling pulse was performed before each experiment (an experiment is defined here as one complete PUND sequence) to ensure a consistent initial microstructure across all experiments. Due to reversibility of polarization switching and to avoid intrinsic sample-to-sample variability, all measurements belonging to one dataset were performed on a single sample. The number of electrical field pulses were sufficiently low to avoid effects of polarization fatigue [56].

3.1. Conventional PUND measurements

The electrical and mechanical hysteresis data from conventional PUND experiments are shown in Fig. 2(b). At least three experiments were performed at each rate. Strain data was not collected at the highest rate of applied electric field (10² MV·m⁻¹·s) due to limitations in time resolution of the imaging system. For each pulse, we refer to the *peak* and *remanent* polarization values as, respectively, the polarization values at the maximum applied electric field during the pulse and at zero electric field after

electrical unloading. Three specific conclusions are drawn here: (i) remanent and peak polarization decrease, (ii) coercive fields increase, and (iii) polarization susceptibility (the slope of the p – e -hysteresis) decrease with increasing loading rate. In addition, strain data reveal a decrease in switching strains with increasing loading rate. These are consistent with previous measurements on cyclic electrical displacement hysteresis data [40].

Results indicate that the collective mobility¹ of polarization switching decreases at higher rates, resulting in incomplete polarization switching at the end of the N and P switching steps. Consequently, the D and U pulses are no longer ‘non-switching’ steps – conventionally used to probe dielectric and sample leakage effects – but involve the evolution of residual polarization from the previous pulse. This prevents using this data to infer microscopic DW kinetics. The ‘apparent’ rate dependence in electro-mechanical switching (see Fig. 2(b)) is not only due to the intrinsic DW kinetics but also due to different initial configurations (i.e., initial domain microstructure) for each pulse. This discrepancy in initial conditions arises from incomplete switching in the previous (N or P) pulses, especially at higher rates. Without the support of direct *in-situ* imaging techniques, the interpretation of rate effects from such data is difficult—the only recourse being coupling experimental data with kinetic models for domain evolution [57]. However, most such models lack accurate kinetics required to describe rate effects at domain length scales and short time scales (see, e.g., the discussion in [35]), a problem we seek to overcome by the modified PUND experiment, to separately understand the effects of initial conditions and rate dependence from macroscopic experimental data. This will be our focus for the remainder of this study.

3.2. Modified PUND measurements

Fig. 3(b) shows data from modified PUND measurements across electric field loading rates spanning five orders of magnitude. At least three experiments were performed at each loading rate; the resulting error bars confirm excellent repeatability. Each column in Fig. 3(b) corresponds to a pulse in the sequence (indicated by the labels). The first row shows the change in electric displacement (d) as a function of the applied electric field (e), also referred to as the d – e -hysteresis loop (a half-loop in this case). The second row presents the total surface strain data measured *in-situ* using stereo-DIC and averaged over the region of interest (referred to as the ϵ – e -loop). As explained in Section 2.5, the modified PUND experiments allow us to calculate the total polarization p and remanent switching strain Δs (otherwise not easily accessible by macroscopic cyclic experiments).

3.2.1. Rate-dependent kinetics of polarization switching

Fig. 4 presents polarization switching data in the form of p – e -hysteresis across all loading rates, calculated from the modified PUND data in Fig. 3(b). Peak and remanent polarization values for each rate are summarized in Fig. 5(a–d).

Pump pulses N show that both peak and remanent polarization values decrease with increasing rate (see Fig. 5(a, c)), confirming rate effects in domain switching: with increasing loading rate, the finite kinetics associated with domain switching increasingly prevent complete switching. This is consistent with prior cyclic measurements [40]. At quasistatic rates, the peak

¹ We use the term *collective mobility* here and in the following as a macroscopic analog of the conventional definition for mobility i.e., the ratio of velocity to driving force on domain walls at the microscale. Contrary to the microscopic definition, collective mobility is not a domain wall property but a function of the domain wall distribution in the sample. This also serves as an intuitive, microstructurally-informed description for polarization susceptibility, used later in the study.

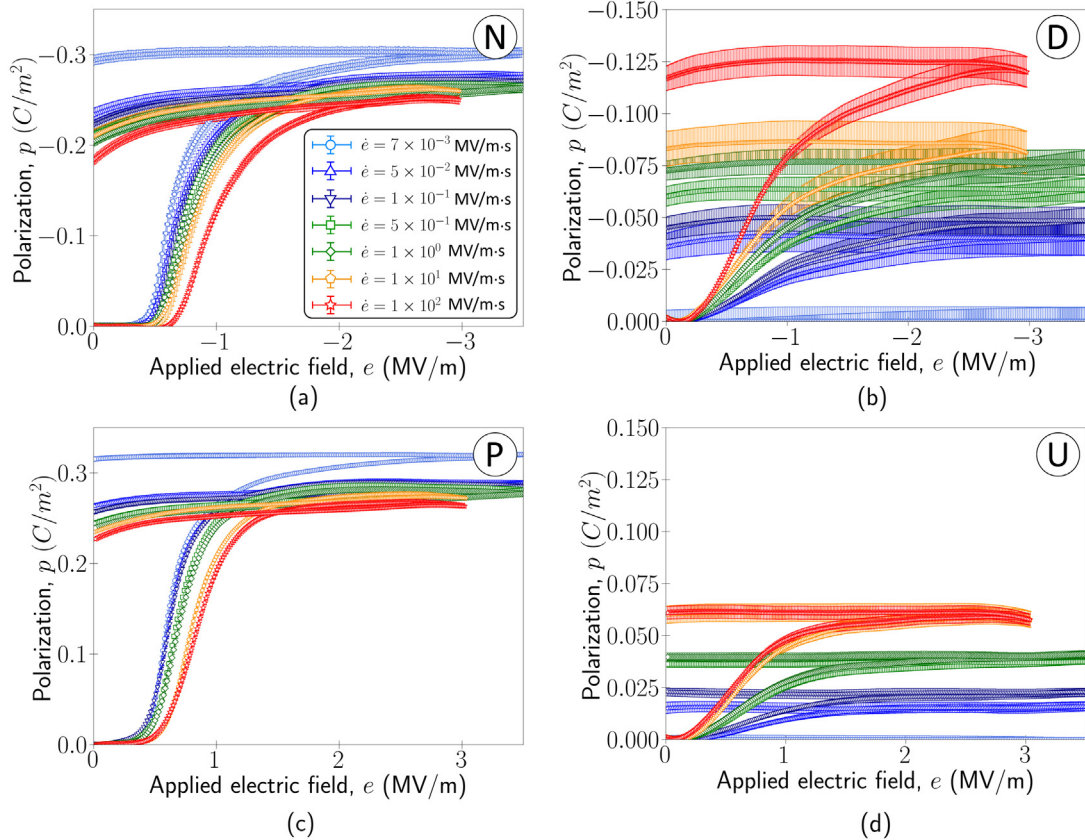


Fig. 4. Polarization p vs. electric field e , extracted from the $d - e$ -data shown in Fig. 3(b).

polarization approximately equals the remanent polarization, indicating irreversible and complete switching. At higher rates, the difference between the peak and remanent polarization values increase. We refer to this as *back-switching*:

$$p_{(b)} = |p_{(pk)} - p_{(r)}|. \quad (9)$$

Physically, back-switching is a measure of the stability of the domain structure at peak applied electric field. Ideally, a gradual removal of the electric field after its peak value only involves dielectric effects, while the domain microstructure is frozen. However, in reality (especially at high rates) some fraction of the switched domains are unstable and hence are recovered (i.e., removed) during removal of the electric field. This effect is observed as back-switching. The impact of these processes on polarization switching are critical in bulk ferroelectric ceramics due to complex domain structures and internal charged defects.

Fig. 6 shows the back-switched polarization as a function of switching rate for the pump pulses. In addition to incomplete switching, this data shows that an increasing fraction of domains is unstable at higher rates, resulting in reversible polarization upon removal of the electric load. As expected, data from probe pulse D in Figs. 4 and 5(b, d) show the opposite trend, i.e., an increase in the switched polarization with increasing rate. Recall that probe pulses drive the *remanent* polarization quasistatically (at $\dot{e}^{(0)} = 7 \times 10^{-3}$ MV/m·s) at the end of a preceding pump pulse. Hence, after a quasistatic N pulse (which effects complete switching), no significant switching is observed during the subsequent D pulse. By contrast, after a fast N pulse (which induces only partial switching), significant switching follows during the subsequent D pulse. The qualitative trends are similar in the positive direction for pulses P and U (see Figs. 4(c, d), 5, and 6), albeit with weaker rate effects.

Fig. 7 summarizes our discussion of the polarization data, which are plotted as bar charts for both the negative (Fig. 7(a)) and positive pulses (Fig. 7(b)). While the total switched polarization remains constant (variation < 10%), hence confirming repeatable complete switching, the ratio between polarization switching during the pump vs. probe pulses increases significantly with electric field loading rate. That is, at the end of each set of ND or PU pulses, the remanent polarization is approximately the same; yet, with increasing rate, the pump pulse effects less stable domain switching, while the subsequent quasistatic probe pulses recovers the increasingly “unswitched” polarization. This is shown schematically in Fig. 7(c, d). Rate effects are less pronounced (but significant) for pulses applied in the positive direction, i.e., parallel to the pre-poled direction. This asymmetry is attributed to the development of internal bias fields due to defects within the ferroelectric ceramic. The effects of this asymmetry will be discussed in detail later.

Fig. 4 also reveals that the slope of the $p - e$ -hysteresis is rate-dependent. We define the polarization susceptibility $\epsilon^p = \partial p / \partial e$ as the (locally varying) slope of the $p - e$ -curve. Physically, ϵ^p is indicative of the collective mobility of domain walls in a volume-averaged sense. It is evident from Fig. 4 and Eq. (3) that ϵ^p is initially zero (dielectric effect), increases to a maximum (during polarization switching), and finally decreases (saturation)—this is in line with measurements of dissipation during the switching process [11]. From a micro-mechanics standpoint, the peak polarization susceptibility is representative of the peak domain activity, contributing to the reversal of volume-averaged polarization (for the pump pulses). While domain activity entails a combination of nucleation and growth of domain walls during the pump pulses N and P, the quasistatic probe pulses D and U are assumed to predominantly cause the growth of existing domain walls. This assumption is justified by the low electrical loading

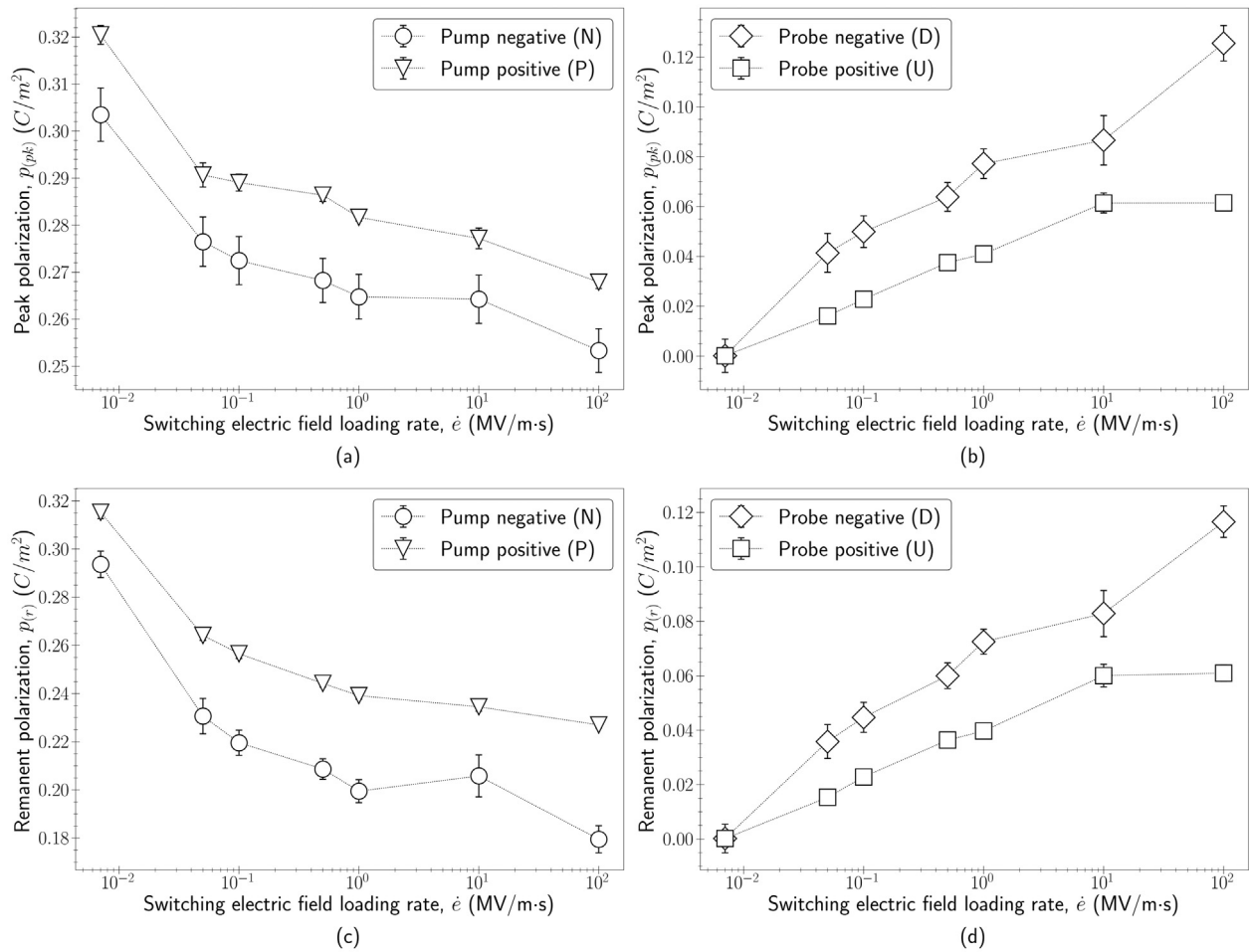


Fig. 5. Peak polarization p_{pk} and remanent polarization p_r as functions of the loading rate for (a, c) pump and (b, d) probe pulses. Note that the switching electric field loading rate refers to the rate of the pump pulses (for probe pulses, the rate of the preceding pump pulse).

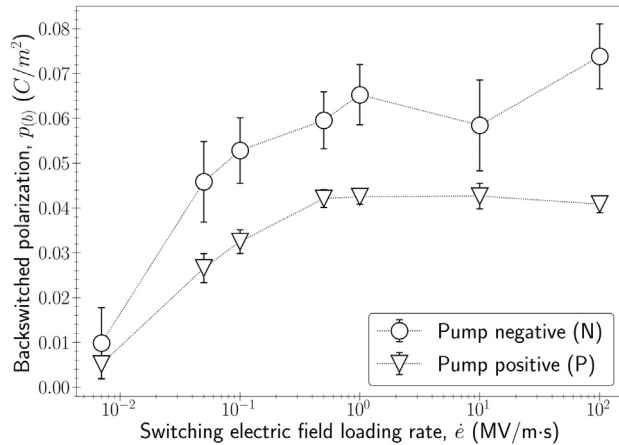


Fig. 6. Back-switched polarization p_b vs. electric field loading rate \dot{e} for the pump pulses.

rates of the D and U pulses as well as the higher energetic cost of domain nucleation vs. of the growth of pre-existing domains.

Fig. 8 shows the peak polarization susceptibility for the pump (Fig. 8a) and probe pulses (Fig. 8b). The apparent decreasing trend with increasing loading rate of the pump pulses (N and P) implies a decrease in the collective mobility of polarization switching (the microscopic kinetic origin of which is unclear from this data

alone). The probe pulses (D and U), however, show an increase in peak polarization susceptibility with the loading rate of the preceding pump pulses. Since all probe pulses were performed at quasistatic rates, this trend is attributed to the migration of a larger density of residual domain walls due to enhanced nucleation during the pump pulses with increasing rate. In other words, at high rates, more domains are being nucleated during the pump pulses, which do not achieve complete switching upon unloading and which respond more readily with DW motion to electric fields applied during the probe pulses.

An analysis of the rate-dependent coercive field supports this picture of the microscopic domain kinetics. We define the *coercive field* e_c as the electric field at which peak polarization susceptibility (or peak domain activity) occurs. Fig. 9 presents e_c as a function of the loading rate from both pump and probe pulses. Data from the pump pulses (Fig. 9a) show a nearly 50% increase in coercive fields (along with decreased polarization and susceptibility). Interestingly, data from the probe pulses (Fig. 9b) show the opposite trend, which is explained as follows. Since no intrinsic rate dependence is expected from the quasistatic probe pulses, the coercive field data is interpreted to indicate an increased density of remanent domain walls (and domain configurations farther from equilibrium) after the pump pulses at higher rates. This further confirms the dominance of domain nucleation over DW motion at high rates.

Let us discuss the asymmetry in the measured hysteresis: all data discussed so far show differences when the electric fields are applied parallel to the pre-poled direction (positive by our

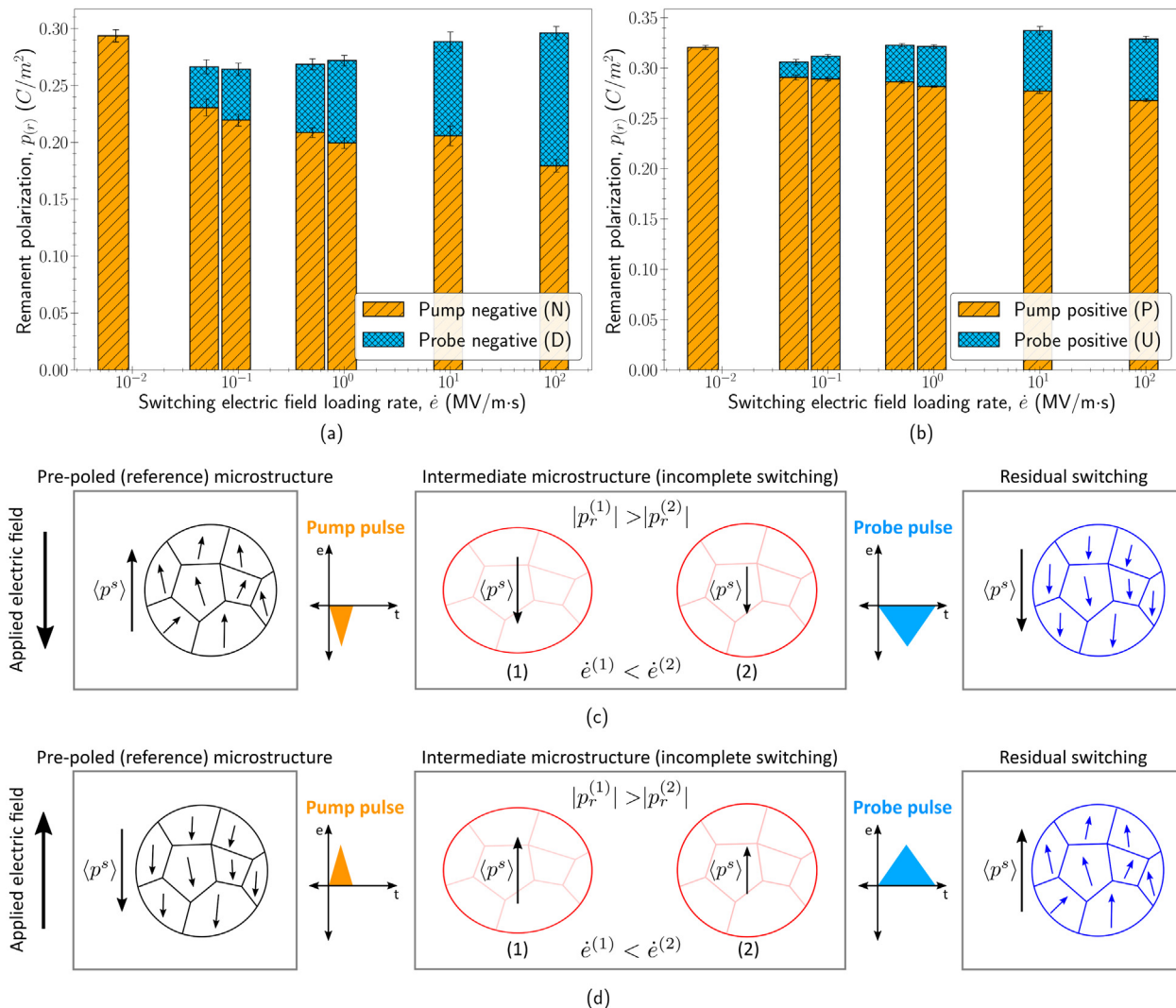


Fig. 7. Remanent polarization p_r of the pump and probe pulses in the (a) negative and (b) positive direction. (c, d) Schematic illustration of the microstructural processes and resulting remanent polarization values during all pulses.

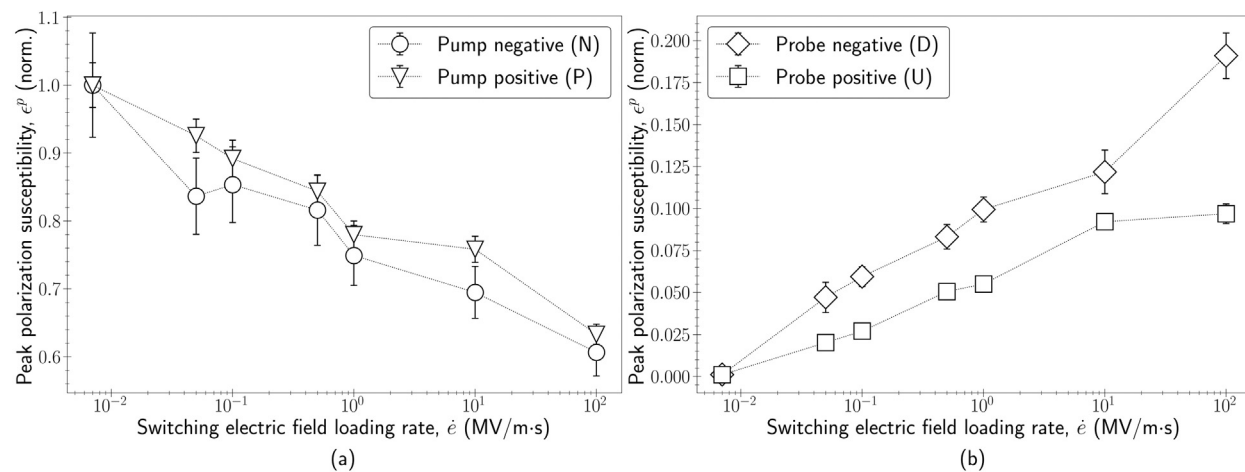


Fig. 8. Peak polarization susceptibility e^p as a function of electric loading rate for (a) pump and (b) probe pulse data. Note that the switching electric field loading rate refers to the rate of the *pump* pulses (for probe pulses, the rate of the preceding pump pulse).

convention; pulses P and U) vs. anti-parallel (negative by our convention; pulses N and D). Evidence of such asymmetry during

cyclic hysteresis measurements, especially in poled and doped ferroelectric ceramics, is abundant in the literature [58–63] and

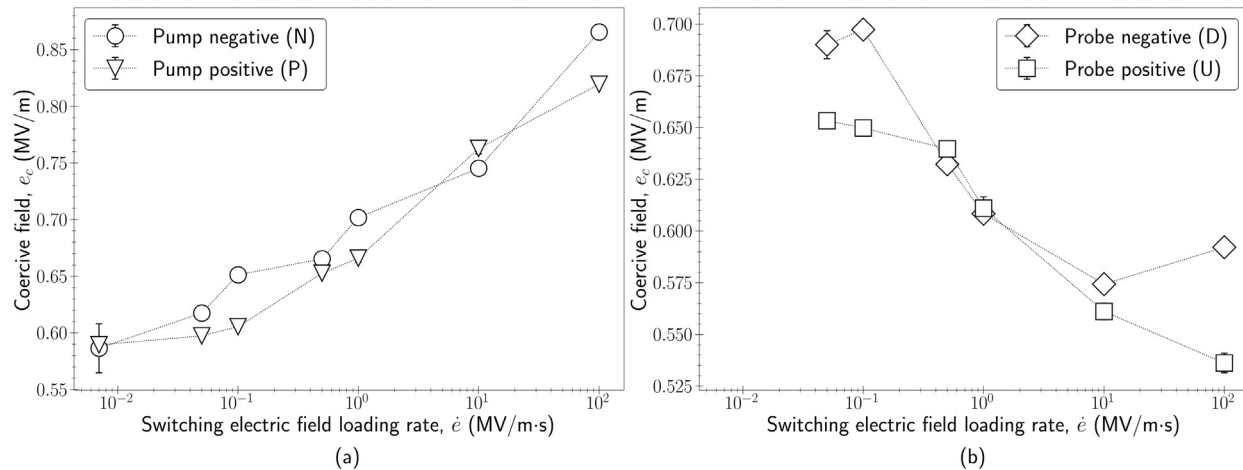


Fig. 9. Coercive field as a function of loading rate from (a) pump; (b) probe data. Note that the switching electric field loading rate refers to the rate of the *pump* pulses (for probe pulses, the rate of the preceding pump pulse).

primarily attributed to defects in the material [64,65]. This leads to an additional mechanism influencing the switching kinetics: the evolution of defect dipoles or space charges. A competition between the time scales of electric loading, of domain wall nucleation and growth, and of defect dipole reorientation hence is responsible for the observed asymmetry and its rate dependence.

Our modified PUND experiments shed light into this competition. The peak polarization during P pulses is greater than during N pulses, while rate effects are comparable. Consistent with that, probe pulses D shows more residual switching compared to U (see Fig. 5(b)). Notice that the difference between D and U data increases with rate (Fig. 5(b)). As we argued before that the rate-dependent polarization susceptibility in probe pulse data is due to an increase in the remanent domain wall density after high-rate pump pulses, the data in Fig. 8(b) suggests that domain nucleation is enhanced when switching anti-parallel to the pre-poled direction. This makes sense when considering that internal bias electric fields arise from defects, which are expected to align more favorably with the pre-poled direction. As a consequence, two effects are evident: (i) the back-switched polarization is higher (Fig. 6), and (ii) domain nucleation at high rates is more pronounced when switching anti-parallel to the bias field—as confirmed by the susceptibility probe data (Fig. 8(b)).

3.2.2. Switching strain as a function of rate: Competition between 90 and 180 degree domain activity

So far we discussed the competition between domain nucleation and growth—without consideration of the type of DWs and domain variants. BaTiO₃ is an ideal material system to address this question due to its purely tetragonal crystallography at room temperature (unlike, e.g., lead zirconate titanate, in which rhombohedral phases may form). In three dimensions, six tetragonal domain variants are feasible, resulting in two types of DWs, classified as ferroelectric (180°) and ferroelastic (90°). The former are characterized by a jump in only the electric dipole moment, while the latter are characterized by jumps in both dipole moment and mechanical strain. Consequently, only ferroelastic domain evolution results in macroscopic switching strains. In other words, the volume-averaged transformation strain s in Eq. (7) is non-zero only during 90° switching or ferroelastic DW activity.

Fig. 10 presents a schematic description for the interpretation of the remanent strain data (note that a volume-averaged/effective polarization is shown for each grain). We consider a polycrystalline ceramic where the polarization of all grains are aligned to represent a poled state. During the pump pulse, incomplete switching may result in an intermediate/residual microstructure

that is representative of either ferroelastic 90° (case 1) or ferroelectric 180° (case 2) domain switching. The difference between the initial and final strains of the sample yields the remanent strain difference Δs . Importantly, this remanent strain is sensitive to changes in volume fraction of only 90° domains, so that $|\Delta s^{(1)}| > |\Delta s^{(2)}|$ in the example shown in Fig. 10. Analogous interpretations hold for the probe pulse data. We hence use the remanent strain data to probe the relative competition between 90° and 180° domains as a function of loading rate.

Figs. 11 and 12 show the remanent strain data during the pump and probe pulses for switching anti-parallel and parallel to the pre-poled direction, along with a schematic representation of the proposed mechanisms. Note that the scatter in data is larger than that in the total strain measurements (Fig. 3(b)) due to limitations in the DIC resolution (on the order of 100 $\mu\epsilon$) [66].

During the negative switching step (N), the pump pulses show a significant increase in the negative remanent strain ($\sim 100\%$) with switching rate (Fig. 11(a)). This is consistent with our previous conclusion of increased domain nucleation (especially of 90° domains) but reduced DW motion with increasing loading rate, hence resulting in significant amounts of residual 90° domain walls after the pump pulse) (see Fig. 11(c)). The probe pulse data (D) shows an increasing trend up to $\dot{e} \simeq 10^0$ MV/m s, which again indicates greater residual 90° domain volume fractions at the end of the preceding pump pulse (Fig. 11(b)). For $\dot{e} > 10^0$ MV/m s, however, the probe pulse data (D) show a decreasing trend. The origin of this non-monotonicity is unclear as yet. We hypothesize that this is an effect of the internal bias fields due to charged and dipolar defects generated during manufacturing. The internal bias field in this case is oriented opposite to the direction of switching and tends to reverse switched domains locally. This is considerably easier when domain sizes are small—a consequence of more pronounced nucleation at higher switching rates. Smaller domains are less stable, causing the internal bias fields to annihilate these ‘unstable’ domains, even when no external field is applied (between the N and D pulses). The back-switched polarization data (Fig. 6) supports this hypothesis.

As a consequence, the total switched polarization along the negative direction is slightly less than that along the positive direction, as shown in Fig. 7. This may imply the presence of few 90° domain walls before applying the P pulse. Remanent strain data for the positive switching step (P) show a different trend (Fig. 12(a)). At low electric field rates, the remanent strains are positive, indicating that the motion of existing 90° domain walls are preferred over nucleation. At higher rates, the remanent strains are negligible, consistent with the conclusion that domain

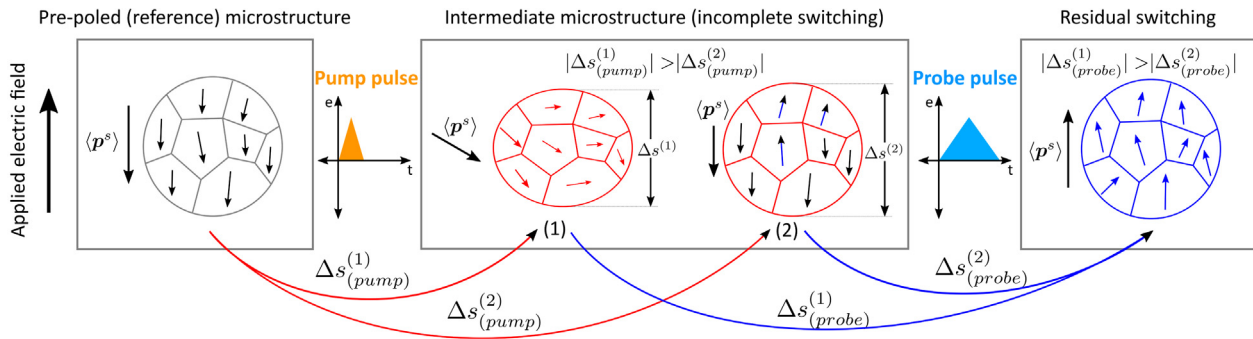


Fig. 10. Schematic representation of the remanent strain due to incomplete switching involving primarily 90° (case 1) vs. 180° switching (case 2).

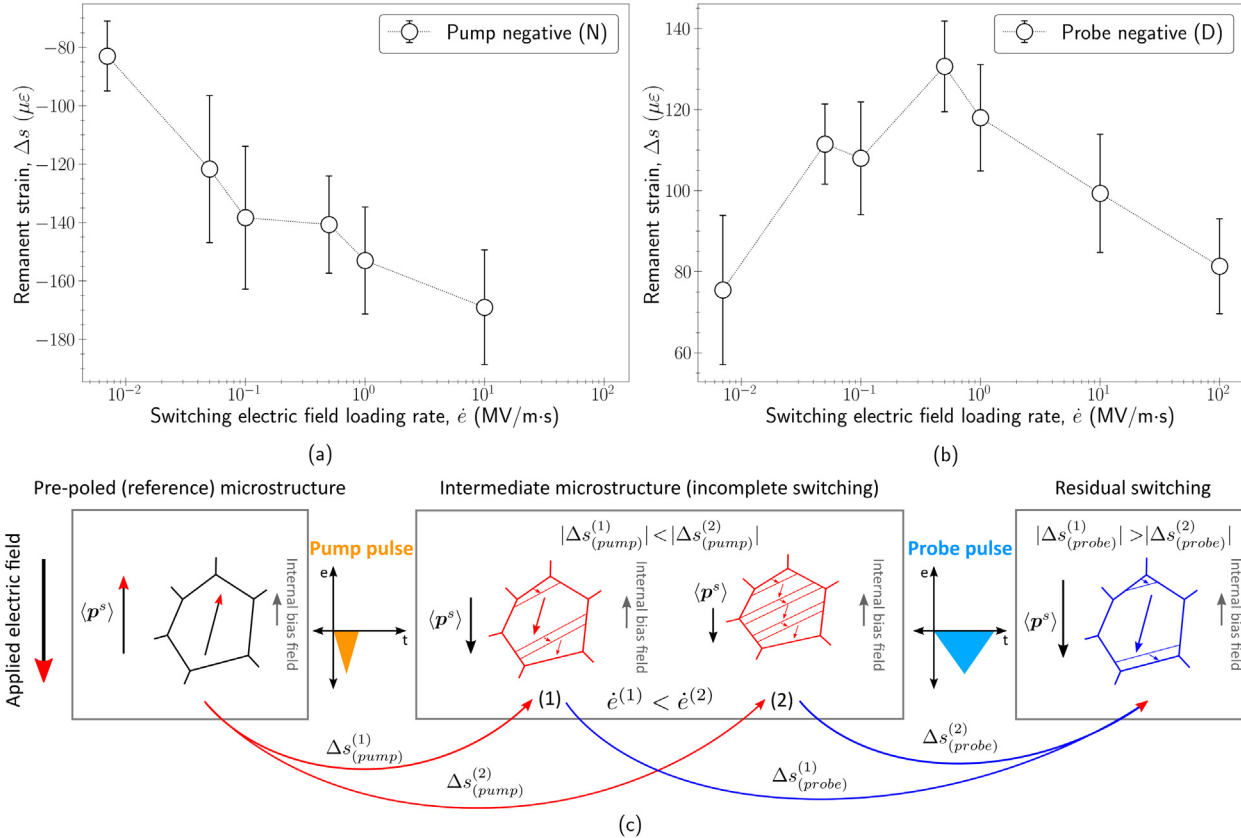


Fig. 11. Remanent strain data during switching anti-parallel to the pre-poled direction: (a) pump and (b) probe pulse data. (c) Schematic description of the proposed switching mechanisms. Note that the switching electric field loading rate refers to the rate of the pump pulses (for probe pulses, this is the rate of the preceding pump pulse).

walls show less motion at higher rates. More importantly, this also shows that the additional nucleation of domain walls are not ferroelastic (90°), as observed during the N pulses, but ferroelectric (180°)—see the schematic in Fig. 12(c). The probe pulse data (U) shows the opposite trend (Fig. 12(b)). At lower rates, a lower fraction of remanent 90° domain walls remain after the pump pulse N. However, the remanent strain (hence remanent 90° domain volume fraction) remains insensitive to rate beyond $\dot{e} = 10^{-1} \text{ MV/m s}$, due to increased nucleation of 180° domains. While the energetic cost of nucleating 180° domains is higher than 90° [31], the internal bias fields may provide the additional driving force.

The strong asymmetry in polarization switching and domain variant selection shows that defect distributions play a crucial role in the rate dependence of polarization switching and microstructural evolution of ferroelectric ceramics. In our material,

the asymmetry of the hysteresis loop was found to evolve with the cycling frequency [40], emphasizing the role of defect kinetics in the study of domain wall kinetics—especially in bulk ferroelectric ceramics. We reiterate that the inherent limitations of the stereo-DIC technique warrant the use of high-resolution interferometry-based methods [67–69] to probe non-linear domain wall kinetics in future experiments [70].

Nevertheless, the stereo-DIC technique presented in this study can be exploited for more detailed descriptions of ferroelastic switching kinetics. Consider the remanent switching strain (Eq. (8)). In our current study, full-field strain data was processed to extract strains along the direction of applied electric field. Knowledge of the full-field switching strain tensor could shed light on the orientation distribution of polarization during 90° ferroelastic switching (which is a complex process ultimately

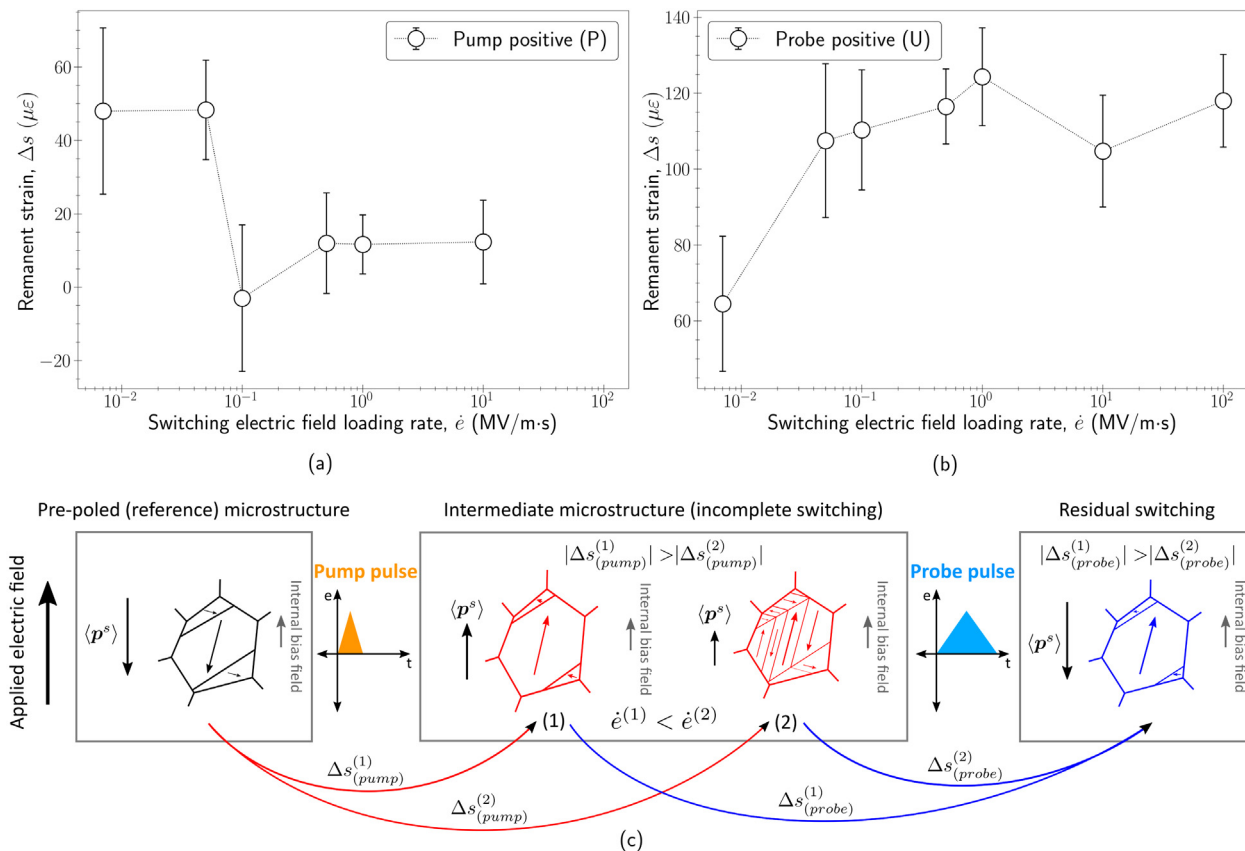


Fig. 12. Remanent strain data during switching parallel to the pre-poled direction: (a) pump and (b) probe pulse data. (c) Schematic description of the proposed switching mechanisms. Note that the switching electric field loading rate refers to the rate of the *pump* pulses (for probe pulses, this is the rate of the preceding *pump* pulse).

involving all six tetragonal variants). A combination of the experimental technique used in this study with detailed texture analysis prior to applying electro-mechanical loading can offer new insight for the calibration and validation of phenomenological models [71–73].

4. Conclusion

We have presented in-situ experiments, which probed the effect of electrical loading rate on electro-mechanical switching in polycrystalline barium titanate. A modification of the traditional Positive Up Negative Down (PUND) experiments allowed us to interpret the kinetics of microstructural domain evolution (indirectly) as a function of rate of the applied electric field. Using pump pulses designed to reverse a poled polarization state at different rates, we quantified the decrease in peak (~20%) and remanent (~40%) polarization from rates of 10^{-2} to 10^2 MV/m·s. These rate effects were weaker during switching parallel vs. anti-parallel to the pre-poled direction. In addition, reversible polarization switching (or back-switching) upon removal of the electric field increased significantly with rate (by ~25% and ~12%, respectively) when switching anti-parallel vs. parallel to the pre-poled direction. With increasing rate during pump pulses, the polarization susceptibility decreased (~40%), whereas the coercive field (~40%) increased. Subsequent quasistatic probe pulses assessed the remanent polarization at the end of each pump pulse and showed a complete recovery of the incomplete polarization switching during the preceding pump pulse at higher rates. The asymmetry of the pump and probe pulse data indicated a preference for switching along the pre-poled direction of the sample. Mechanical strains were measured in situ during

electrical loading by stereo-DIC, giving evidence of ferroelastic vs. ferroelectric domain switching. During switching anti-parallel to the pre-poled direction, remanent strains were negative for pump pulse data, and increased in magnitude (~100%) with loading rate. During switching parallel to the pre-poled direction, remanent strains were positive at low rates and negligible at high rates.

Our experimental data indicate that, as the electric field loading rate increases, (i) domain nucleation dominates over domain wall motion as the primary switching mechanisms due to the finite relaxation times of domain wall motion, (ii) the density of remanent domain walls increases, (iii) the remanent domain configurations are less stable, leading to more back-switching upon electric field removal, (iv) when switching anti-parallel to the pre-poled direction, 90° domains nucleate increasingly with rate (which are removable during the quasistatic probe pulses), (v) when switching parallel to the pre-poled direction, the microstructural evolution changes from primarily 90° domain wall motion at low rates to 180° domain nucleation at high rates. Overall, rate effects and back-switching were more pronounced during loading anti-parallel to the pre-poled direction. This asymmetry of the pump and probe pulse data stems from internal bias fields (due to defects), which cause a preference for switching along the pre-poled direction of the sample.

Declaration of competing interest

The authors declare the following financial interests/personal relationships which may be considered as potential competing interests: Dennis M. Kochmann has patent Broadband Electromechanical Spectroscopy assigned to the California Institute of Technology.

Statement of data availability

The data that support the findings of this study are available in the ETH Zürich Research Collection under the doi: <https://doi.org/10.3929/ethz-b-000558108>.

Acknowledgments

The authors acknowledge the support from the Swiss National Science Foundation, Switzerland (SNSF project number 200021-178747) and thank L. Guin and R. Indergand for fruitful discussions.

References

- [1] R.W. Whatmore, P.C. Osbond, N.M. Shorrocks, Ferroelectric materials for thermal IR detectors, *Ferroelectrics* 76 (1) (1987) 351–367, <http://dx.doi.org/10.1080/00150198708016956>.
- [2] R. Watton, Ferroelectric materials and devices in infrared detection and imaging, *Ferroelectrics* 91 (1) (1989) 87–108, <http://dx.doi.org/10.1080/00150198908015731>.
- [3] C.R. Bowen, H.A. Kim, P.M. Weaver, S. Dunn, Piezoelectric and ferroelectric materials and structures for energy harvesting applications, *Energy Environ. Sci.* 7 (1) (2014) 25–44, <http://dx.doi.org/10.1039/c3ee42454e>, URL www.rsc.org/ees.
- [4] K.T. Butler, J.M. Frost, A. Walsh, Ferroelectric materials for solar energy conversion: Photoferroics revisited, *Energy Environ. Sci.* 8 (3) (2015) 838–848, <http://dx.doi.org/10.1039/c4ee03523b>, arXiv:1412.6929, URL www.rsc.org/ees.
- [5] T.Y. Kim, S.K. Kim, S.W. Kim, Application of ferroelectric materials for improving output power of energy harvesters, *Nano Converg.* 5 (1) (2018) 1–16, <http://dx.doi.org/10.1186/s40580-018-0163-0>, <https://link.springer.com/articles/10.1186/s40580-018-0163-0>.
- [6] D. Damjanovic, P. Muralt, N. Setter, Ferroelectric sensors, *IEE Sensors J.* 1 (3) (2001) 191–206.
- [7] E.F. Crawley, J. De Luis, Use of piezoelectric actuators as elements of intelligent structures, *AIAA J.* 25 (10) (1986) 1373–1385, <http://dx.doi.org/10.2514/3.9792>, URL <http://arc.aiaa.org>.
- [8] T.A. Asare, B.D. Poquette, J.P. Schultz, S.L. Kampe, Investigating the vibration damping behavior of barium titanate (BaTiO_3) ceramics for use as a high damping reinforcement in metal matrix composites, *J. Mater. Sci.* 47 (6) (2012) 2573–2582, <http://dx.doi.org/10.1007/s10853-011-6080-9>, URL <https://link.springer.com/article/10.1007/s10853-011-6080-9>.
- [9] K.P. Duffy, B.B. Choi, A.J. Provenza, J.B. Min, N. Kray, Active piezoelectric vibration control of subscale composite fan blades, *J. Eng. Gas Turbines Power* 135 (1) (2013) <http://dx.doi.org/10.1115/1.4007720>, URL http://asmedigitalcollection.asme.org/gasturbinespower/article-pdf/135/1/011601/6155908/gtp_135_1_011601.pdf.
- [10] K. Patterson, Lightweight deformable mirrors for future space telescopes (Ph.D. thesis), California Institute of Technology, 2013, <http://dx.doi.org/10.7907/S7JS-A837>.
- [11] C.S. Wojnar, J.-B. le Graverend, D.M. Kochmann, Broadband control of the viscoelasticity of ferroelectrics via domain switching, *Appl. Phys. Lett.* 105 (16) (2014) 162912, <http://dx.doi.org/10.1063/1.4899055>, URL <http://aip.scitation.org/doi/full/10.1063/1.4899055>.
- [12] V.I. Pilipovich, V.I. Polyakov, A.I. Konoiko, Electro-optic light modulators, *Instruments Exp. Tech. New York* 30 (1 pt 2) (1987) 199–201, <http://dx.doi.org/10.1364/ao.5.001612>, URL <https://www.osapublishing.org/viewmedia.cfm?uri=ao-5-10-1612&seq=0&html=true>, <https://www.osapublishing.org/abstract.cfm?uri=ao-5-10-1612>, <https://www.osapublishing.org/ao/abstract.cfm?uri=ao-5-10-1612>.
- [13] D.A. Buck, Ferroelectrics for digital information storage and switching, *Tech. rep.*, 1952, <http://hdl.handle.net/1721.3/40244>.
- [14] Y. Tarui, T. Hirai, K. Teramoto, H. Koike, K. Nagashima, Application of the ferroelectric materials to ULSI memories, *Appl. Surf. Sci.* 113–114 (1997) 656–663, [http://dx.doi.org/10.1016/S0169-4332\(96\)00963-4](http://dx.doi.org/10.1016/S0169-4332(96)00963-4).
- [15] O. Auciello, R. Ramesh, The physics of ferroelectric memories, *Phys. Today* (1998) 22–27, URL <https://www.researchgate.net/publication/273629413>.
- [16] J.A. Mundy, J. Schaab, Y. Kumagai, A. Cano, M. Stengel, I.P. Krug, D.M. Gottlob, H. Doğanay, M.E. Holtz, R. Held, Z. Yan, E. Bourret, C.M. Schneider, D.G. Schlom, D.A. Muller, R. Ramesh, N.A. Spaldin, D. Meier, Functional electronic inversion layers at ferroelectric domain walls, *Nat. Mater.* 16 (6) (2017) 622–627, <http://dx.doi.org/10.1038/nmat4878>, URL <https://www.nature.com/articles/nmat4878>.
- [17] J. Schaab, S.H. Skjærøv, S. Krohns, X. Dai, M.E. Holtz, A. Cano, M. Lilienblum, Z. Yan, E. Bourret, D.A. Muller, M. Fiebig, S.M. Selbach, D. Meier, Electrical half-wave rectification at ferroelectric domain walls, *Nat. Nanotechnol.* 13 (11) (2018) 1028–1034, <http://dx.doi.org/10.1038/s41565-018-0253-5>, URL <https://www.nature.com/articles/s41565-018-0253-5>.
- [18] B. Jaffe, W.R. Cook Jr., H. Jaffe, *Piezoelectric Ceramics*, Elsevier, 1971, <http://dx.doi.org/10.1016/B978-0-12-379550-2.X5001-7>, URL <https://linkinghub.elsevier.com/retrieve/pii/B9780123795502X50017>.
- [19] D. Meier, J. Seidel, M. Gregg, R. Ramesh, *Domain Walls*, Oxford University Press, 2020, <http://dx.doi.org/10.1093/oso/bf0198862499.001.0001>.
- [20] D. Viehland, Y.-H. Chen, Random-field model for ferroelectric domain dynamics and polarization reversal, *J. Appl. Phys.* 88 (11) (2000) 6696–6707, <http://dx.doi.org/10.1063/1.1325001>.
- [21] D. Zhou, M. Kamlah, D. Munz, Rate dependence of soft PZT ceramics under electric field loading, in: C.S. Lynch (Ed.), *Smart Struct. Mater.* 2001 Act. Mater. Behav. Mech., (11) SPIE, 2001, p. 64, <http://dx.doi.org/10.1117/12.432740>, URL <http://proceedings.spiedigitallibrary.org/proceeding.aspx?doi=10.1117/12.432740>.
- [22] A. Achuthan, C.T. Sun, A study of mechanisms of domain switching in a ferroelectric material via loading rate effect, *Acta Mater.* 57 (13) (2009) 3868–3875, <http://dx.doi.org/10.1016/j.actamat.2009.04.043>.
- [23] M.H. Lente, A. Picinin, J.P. Rino, J.A. Eiras, 90° domain wall relaxation and frequency dependence of the coercive field in the ferroelectric switching process, *J. Appl. Phys.* 95 (2004) 2646–2653, <http://dx.doi.org/10.1063/1.1645980>, URL <http://aip.scitation.org/doi/10.1063/1.1645980>.
- [24] R. Yimnirun, Y. Laosirithaworn, S. Wongsaenmai, S. Ananta, Scaling behavior of dynamic hysteresis in soft lead zirconate titanate bulk ceramics, *Appl. Phys. Lett.* 89 (16) (2006) 162901, <http://dx.doi.org/10.1063/1.2363143>.
- [25] J. Yin, W. Cao, Coercive field of the $0.95\text{Pb}(\text{Zn}_1/3\text{Nb}_2/3)\text{O}_3 - 0.045\text{PbTiO}_3$ single crystal and its frequency dependence, *Appl. Phys. Lett.* 80 (6) (2002) 1043–1045, <http://dx.doi.org/10.1063/1.1448385>.
- [26] Q.M. Zhang, W.Y. Pan, S.J. Jang, L.E. Cross, Domain wall excitations and their contributions to the weak-signal response of doped lead zirconate titanate ceramics, *J. Appl. Phys.* 64 (11) (1988) 6445–6451, <http://dx.doi.org/10.1063/1.342059>.
- [27] A. Pramanick, A.D. Prewitt, J.S. Forrester, J.L. Jones, Domains, domain walls and defects in perovskite ferroelectric oxides: A review of present understanding and recent contributions, *Crit. Rev. Solid State Mater. Sci.* 37 (4) (2012) 243–275, <http://dx.doi.org/10.1080/10408436.2012.686891>.
- [28] T. Iamsasri, G. Esteves, H. Choe, M. Vogt, S. Prasertpalichat, D.P. Cann, S. Gorfman, J.L. Jones, Time and frequency-dependence of the electric field-induced phase transition in $\text{BaTiO}_3\text{-BiZn}_1/2\text{Ti}_1/2\text{O}_3$, *J. Appl. Phys.* 122 (6) (2017) 064104, <http://dx.doi.org/10.1063/1.4998163>.
- [29] S. Gorfman, H. Simons, T. Iamsasri, S. Prasertpalichat, D.P. Cann, H. Choe, U. Pietsch, Y. Watier, J.L. Jones, Simultaneous resonant x-ray diffraction measurement of polarization inversion and lattice strain in polycrystalline ferroelectrics, *Sci. Rep.* 6 (2016) 20829, <http://dx.doi.org/10.1038/srep20829>.
- [30] W.J. Merz, Domain formation and domain wall motions in ferroelectric BaTiO_3 single crystals, *Phys. Rev.* 95 (3) (1954) 690–698, <http://dx.doi.org/10.1103/PhysRev.95.690>.
- [31] E.A. Little, Dynamic behavior of domain walls in barium titanate, *Phys. Rev.* 98 (4) (1955) 978–984, <http://dx.doi.org/10.1103/PhysRev.98.978>, URL <https://journals.aps.org/pr/abstract/10.1103/PhysRev.98.978>.
- [32] J. Schultheiß, L. Liu, H. Kungl, M. Weber, L. Kodumudi Venkataraman, S. Checchia, D. Damjanovic, J.E. Daniels, J. Koruda, Revealing the sequence of switching mechanisms in polycrystalline ferroelectric/ferroelastic materials, *Acta Mater.* 157 (2018) 355–363, <http://dx.doi.org/10.1016/j.actamat.2018.07.018>.
- [33] A.K. Tagantsev, L. Fousek, Domains in Ferroic Crystals and Thin Films, Springer New York, 2010, pp. 1–819, <http://dx.doi.org/10.1007/978-1-4419-1417-0>.
- [34] T. Yang, B. Wang, J.-M. Hu, L.-Q. Chen, Domain dynamics under ultrafast electric-field pulses, *Phys. Rev. Lett.* 124 (2020) 107601, <http://dx.doi.org/10.1103/PhysRevLett.124.107601>, URL <https://link.aps.org/doi/10.1103/PhysRevLett.124.107601>.
- [35] L. Guin, D.M. Kochmann, A phase-field model for ferroelectrics with general kinetics. part i: Model formulation (submitted), 2022, <http://dx.doi.org/10.48550/ARXIV.2203.16479>, URL <https://arxiv.org/abs/2203.16479>.
- [36] J.E. Daniels, A. Pramanick, J.L. Jones, Time-resolved characterization of ferroelectrics using high-energy X-Ray diffraction, *IEEE Trans. Ultrason. Ferroelectr. Freq. Control* 56 (8) (2009) 1539–1545, <http://dx.doi.org/10.1109/TUFFC.2009.1218>.
- [37] J.E. Daniels, C. Cozzani, S. Ukitrunkun, G. Tutuncu, J. Andrieux, J. Glaum, C. Dosch, W. Jo, J.L. Jones, Two-step polarization reversal in biased ferroelectrics, *J. Appl. Phys.* 115 (22) (2014) 224104, <http://dx.doi.org/10.1063/1.4881835>.
- [38] K.M. Rabe, M. Dawber, C. Lichtensteiger, C.H. Ahn, J.-M. Triscone, Modern physics of ferroelectrics: Essential background, in: *Physics of Ferroelectrics: A Modern Perspective*, Springer Berlin Heidelberg, Berlin, Heidelberg, 2007, pp. 1–30, http://dx.doi.org/10.1007/978-3-540-34591-6_1.
- [39] J.B. le Graverend, C.S. Wojnar, D.M. Kochmann, Broadband electromechanical spectroscopy: characterizing the dynamic mechanical response of viscoelastic materials under temperature and electric field control in a vacuum environment, *J. Mater. Sci.* 50 (10) (2015) 3656–3685, <http://dx.doi.org/10.1007/s10853-015-8928-x>, URL <https://link.springer.com/article/10.1007/s10853-015-8928-x>.

- [40] V. Kannan, M. Trasslin, D.M. Kochmann, Kinetics of ferroelectric switching in poled barium titanate ceramics: effects of electrical cycling rate, *Materialia* 25 (2022) 101553, <http://dx.doi.org/10.1016/j.mtla.2022.101553>, <https://www.sciencedirect.com/science/article/pii/S2589152922002356>.
- [41] M.G. Cain, Characterisation of Ferroelectric Bulk Materials and Thin Films, Springer, 2014, <http://dx.doi.org/10.1007/978-1-4020-9311-1>.
- [42] B. Nagaraj, S. Aggarwal, T.K. Song, T. Sawhney, R. Ramesh, Leakage current mechanisms in lead-based thin-film ferroelectric capacitors, *Phys. Rev. B* 59 (1999) 16022–16027, <http://dx.doi.org/10.1103/PhysRevB.59.16022>, URL <https://link.aps.org/doi/10.1103/PhysRevB.59.16022>.
- [43] D.J. Kim, J.Y. Jo, Y.S. Kim, Y.J. Chang, J.S. Lee, J.-G. Yoon, T.K. Song, T.W. Noh, Polarization relaxation induced by a depolarization field in ultrathin ferroelectric BaTiO₃ capacitors, *Phys. Rev. Lett.* 95 (2005) 237602, <http://dx.doi.org/10.1103/PhysRevLett.95.237602>, URL <https://link.aps.org/doi/10.1103/PhysRevLett.95.237602>.
- [44] I. Fina, L. Fàbrega, E. Langenberg, X. Martí, F. Sánchez, M. Varela, J. Fontcuberta, Nonferroelectric contributions to the hysteresis cycles in manganite thin films: A comparative study of measurement techniques, *J. Appl. Phys.* 109 (7) (2011) 074105, <http://dx.doi.org/10.1063/1.3555098>.
- [45] M. Si, X. Lyu, P.R. Shrestha, X. Sun, H. Wang, K.P. Cheung, P.D. Ye, Ultrafast measurements of polarization switching dynamics on ferroelectric and anti-ferroelectric hafnium zirconium oxide, *Appl. Phys. Lett.* 115 (7) (2019) 072107, <http://dx.doi.org/10.1063/1.5098786>.
- [46] Z. Gao, S. Lyu, H. Lyu, Frequency dependence on polarization switching measurement in ferroelectric capacitors, *J. Semicond.* 43 (2022) 014102, <http://dx.doi.org/10.1088/1674-4926/43/1/014102>, URL <http://www.jos.ac.cn/en/article/doi/10.1088/1674-4926/43/1/014102>.
- [47] G. Tas, R.J. Stoner, H.J. Maris, G.W. Rubloff, G.S. Oehrlein, J.M. Halbout, Noninvasive picosecond ultrasonic detection of ultrathin interfacial layers: CFx at the Al/Si interface, *Appl. Phys. Lett.* 61 (15) (1992) 1787–1789, <http://dx.doi.org/10.1063/1.108427>.
- [48] H. Maris, Picosecond ultrasonics, *Sci. Am.* 278 (1) (1998) 86–89, URL <http://www.jstor.org/stable/26057627>.
- [49] J.P. Feser, J. Liu, D.G. Cahill, Pump-probe measurements of the thermal conductivity tensor for materials lacking in-plane symmetry, *Rev. Sci. Instrum.* 85 (10) (2014) 104903, <http://dx.doi.org/10.1063/1.4897622>.
- [50] S. Rezazadeh-Kalehbasti, L.W. Liu, H.J. Maris, P.R. Guduru, In situ measurement of phase bound kinetics during initial lithiation of crystalline silicon through picosecond ultrasonics, *Exp. Mech.* 59 (2019) 681, <http://dx.doi.org/10.1007/s11340-018-00460-5>.
- [51] F. Pérez-Cota, R. Fuentes-Domínguez, S. La Cavera, W. Hardiman, M. Yao, K. Setchfield, E. Moradi, S. Naznin, A. Wright, K.F. Webb, A. Huett, C. Friel, V. Sottile, H.M. Elsheikha, R.J. Smith, M. Clark, Picosecond ultrasonics for elasticity-based imaging and characterization of biological cells, *J. Appl. Phys.* 128 (16) (2020) 160902, <http://dx.doi.org/10.1063/5.0023744>.
- [52] B. Jaffe, W.R. Cook, H. Jaffe, Barium titanate, in: *Piezoelectric Ceram.*, Elsevier, 1971, pp. 53–114, <http://dx.doi.org/10.1016/b978-0-12-379550-2.50009-0>.
- [53] A. Sigov, Y. Podgorny, K. Vorotilov, A. Vishnevskiy, Leakage currents in ferroelectric thin films, *Phase Transit.* 86 (11) (2013) 1141–1151, <http://dx.doi.org/10.1080/01411594.2013.790033>.
- [54] J.F. Scott, Ferroelectrics go bananas, *J. Phys.: Condens. Matter* 20 (2) (2007) 021001, <http://dx.doi.org/10.1088/0953-8984/20/02/021001>.
- [55] M.I. Morozov, D. Damjanovic, Charge migration in ceramics and its relation to ageing, hardening, and softening, *J. Appl. Phys.* 107 (2010) 34106, <http://dx.doi.org/10.1063/1.3284954>.
- [56] W.L. Tan, K.T. Faber, D.M. Kochmann, In-situ observation of evolving microstructural damage and associated effective electro-mechanical properties of PZT during bipolar electrical fatigue, *Acta Mater.* 164 (2019) 704–713, <http://dx.doi.org/10.1016/j.actamat.2018.10.065>, URL <https://www.sciencedirect.com/science/article/pii/S1359645418308759>.
- [57] R. Indergand, A. Vidyasagar, N. Nadkarni, D.M. Kochmann, A phase-field approach to studying the temperature-dependent ferroelectric response of bulk polycrystalline PZT, *J. Mech. Phys. Solids* 144 (2020) 104098, <http://dx.doi.org/10.1016/j.jmps.2020.104098>.
- [58] H.G. Baerwald, D.A. Berlincourt, Electromechanical response and dielectric loss of prepolarized barium titanate under maintained electric bias. Part I, *J. Acoust. Soc. Am.* 25 (4) (1953) 703–710, <http://dx.doi.org/10.1121/1.1907164>.
- [59] M. Takahashi, Space charge effect in lead zirconate titanate ceramics caused by the addition of impurities, *Japan. J. Appl. Phys.* 9 (10) (1970) 1236–1246, <http://dx.doi.org/10.1143/JJAP.9.1236>, <https://iopscience.iop.org/article/10.1143/JJAP.9.1236/meta>.
- [60] H. Thomann, Stabilization effects in piezoelectric lead titanate zirconate ceramics, *Ferroelectrics* 4 (1) (1972) 141–146, <http://dx.doi.org/10.1080/00150197208235755>.
- [61] K. Carl, K.H. Hardtl, Electrical after-effects in Pb(Ti, Zr)O₃ ceramics, *Ferroelectrics* 17 (1) (1977) 413–486, <http://dx.doi.org/10.1080/00150197808236770>.
- [62] P.V. Lambeck, G.H. Jonker, The nature of domain stabilization in ferroelectric perovskites, *J. Phys. Chem. Solids* 47 (5) (1986) 453–461, [http://dx.doi.org/10.1016/0022-3697\(86\)90042-9](http://dx.doi.org/10.1016/0022-3697(86)90042-9).
- [63] H. Neumann, G. Arlt, The deformation of hysteresis curves by an internal bias in ferroelectric ceramics, in: *Ultrason. Symp., IEEE*, 1987, pp. 671–674, URL <https://ieeexplore.ieee.org/stamp/stamp.jsp?arnumber=1535983&tag=1>.
- [64] I.B. Misirlioglu, M.B. Okatan, S.P. Alpay, Effect of asymmetrical interface charges on the hysteresis and domain configurations of ferroelectric thin films, 126, (1) 2011, pp. 142–154, <http://dx.doi.org/10.1080/10584587.2011.575017>, URL <https://www.tandfonline.com/doi/abs/10.1080/10584587.2011.575017>.
- [65] X.L. Wang, B. Li, X.L. Zhong, Y. Zhang, J.B. Wang, Y.C. Zhou, Effects of space charge distribution on ferroelectric hysteresis loops considering the inhomogeneous built-in electric field: A phase field simulation, *J. Appl. Phys.* 112 (11) (2012) 114103, <http://dx.doi.org/10.1063/1.4767702>, URL <https://aip.scitation.org/doi/abs/10.1063/1.4767702>.
- [66] H. Schreier, J.J. Orteu, M.A. Sutton, *Image Correlation for Shape, Motion and Deformation Measurements: Basic Concepts, Theory and Applications*, Springer US, 2009, <http://dx.doi.org/10.1007/978-0-387-78747-3>, URL <https://link.springer.com/book/10.1007/978-0-387-78747-3#toc>.
- [67] A.L. Khoklin, C. Wüthrich, D.V. Taylor, N. Setter, Interferometric measurements of electric field-induced displacements in piezoelectric thin films, *Rev. Sci. Instrum.* 67 (5) (1996) 1935–1941, <http://dx.doi.org/10.1063/1.1147000>.
- [68] L. Lian, N.R. Sottos, Effects of thickness on the piezoelectric and dielectric properties of lead zirconate titanate thin films, *J. Appl. Phys.* 87 (8) (2000) 3941–3949, <http://dx.doi.org/10.1063/1.372439>.
- [69] P. Gerber, A. Roelofs, O. Lohse, C. Kügeler, S. Tiedke, U. Böttger, R. Waser, Short-time piezoelectric measurements in ferroelectric thin films using a double-beam laser interferometer, *Rev. Sci. Instrum.* 74 (4) (2003) 2613–2615, <http://dx.doi.org/10.1063/1.1544415>.
- [70] S. Trolier-McKinstry, N. Bassiri Gharb, D. Damjanovic, Piezoelectric non-linearity due to motion of 180° domain walls in ferroelectric materials at subcoercive fields: A dynamic poling model, *Appl. Phys. Lett.* 88 (20) (2006) 202901, <http://dx.doi.org/10.1063/1.2203750>.
- [71] J. Huber, N. Fleck, C. Landis, R. McMeeking, A constitutive model for ferroelectric polycrystals, *J. Mech. Phys. Solids* 47 (8) (1999) 1663–1697, [http://dx.doi.org/10.1016/S0022-5096\(98\)00122-7](http://dx.doi.org/10.1016/S0022-5096(98)00122-7), URL <https://www.sciencedirect.com/science/article/pii/S0022509698001227>.
- [72] W.L. Tan, D.M. Kochmann, An effective constitutive model for polycrystalline ferroelectric ceramics: Theoretical framework and numerical examples, *Comput. Mater. Sci.* 136 (2017) 223–237, <http://dx.doi.org/10.1016/j.commatsci.2017.04.032>.
- [73] M.I. Idiart, C.J. Bottero, A phenomenological constitutive theory for polycrystalline ferroelectric ceramics based on orientation distribution functions, *Eur. J. Mech. A Solids* 82 (2020) 103982, <http://dx.doi.org/10.1016/j.euromechsol.2020.103982>, URL <https://www.sciencedirect.com/science/article/pii/S099775381930717X>.